Model investigations of Larsen B Ice Shelf dynamics prior to the breakup

H. Sandhäger, W. Rack, and D. Jansen

Alfred-Wegener-Institut für Polar- und Meeresforschung, Postfach 120161, D-27515 Bremerhaven

Introduction

The Larsen B Ice Shelf at the northeast coast of the Antarctic Peninsula (Fig. 1 a) has undergone substantial changes during the last two decades due to regional atmospheric warming (Vaughan and Doake, 1996; Rott et al., 1996; 1998; Skvarca et al., 1998; 1999; Rack et al., 1999; 2000; Rack, 2000; Scambos et al., 2000; 2004 ; Rack and Rott, 2004). The comprehensive documentation of the Larsen B evolution provides important aspects for ice shelf modelling. Observations indicate that all evolution stages from initially stable configuration over gradual retreat to rapid collapse of the northern and central ice shelf parts (Fig. 1 b) were decisively affected by fracture processes. This accentuates the need for expanding conventional ice shelf model approaches to consider the relevance of fracturing. Furthermore, retreat and disintegration of Larsen B were found to be preceded by noticeable changes in the flow and stress regimes of the ice body (Rott et al., 1998; Skvarca et al., 1999; Rack, 2000; Rack and Rott, 2004). Thus, model experiments on these changes in ice dynamics could contribute to gain better insight into the mechanisms of climate-induced ice shelf break-up. One of the key processes appears to be fracturing enhanced by abundant surface melt due to increasing air temperatures (Skvarca et al., 1999; Scambos et al., 2000; 2004; Rack and Rott, 2004). Another aspect to be mentioned is the potential of the Larsen B database to supply reliable model input data and enable detailed validation of model results.

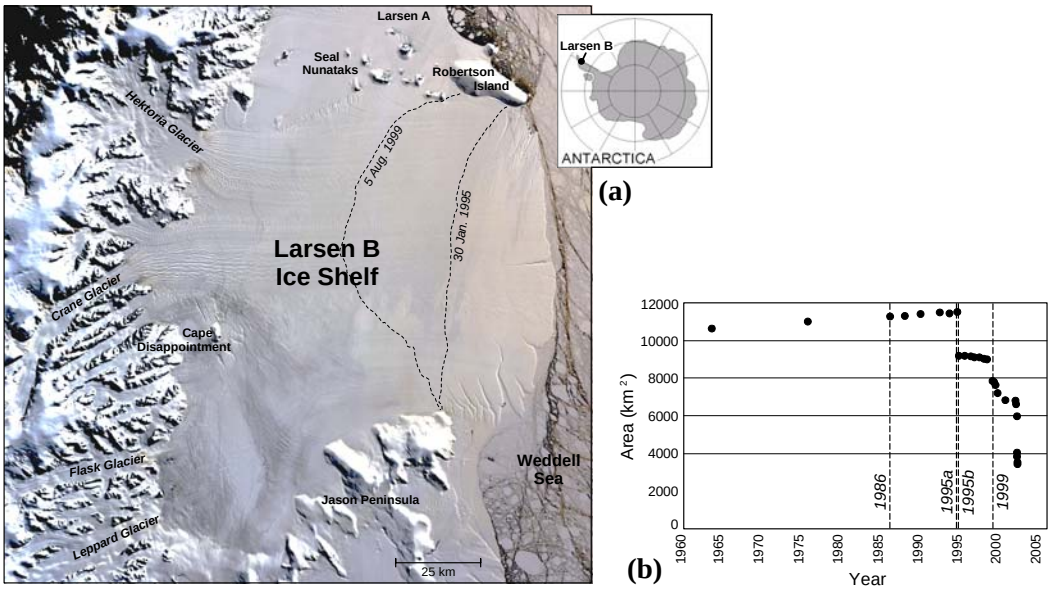

Figure 1: (**a**) Landsat MSS image showing the 1986 configuration of Larsen B Ice Shelf and parts of its catchment area with distinct glacier systems. Indicated ice front positions of the 1995 post-calving stage and the gradually retreating ice shelf in 1999 are also considered in the numerical experiments. These do not yet include the collapse of the northern and central Larsen B sections in February / March 2002. (**b**) Time series of Larsen B Ice Shelf area. Dates assigned to the numerical experiments are marked.

Our investigations aim at expanding an ice flow model based on conventional approaches and attaining an adequate simulation of the ice dynamics of Larsen B in its former stable configuration. The corresponding Configuration Run for the 1986 ice shelf stage yielded considerably more appropriate results than our Reference Run with the ordinary model approach. This gave us reason to perform a series of numerical experiments for the subsequent period of successive ice shelf retreat. Sensitivity Runs were carried out for the Larsen B stages directly prior to and after the major calving event in January 1995, as well as for the August 1999 stage with largely retreated ice front position (Fig. 1).

Description and setup of the numerical flow model

The advancement of the finite difference flow model COMB*IS*^{2}S (Computer-based Ice Shelf / Ice Sheet Simulator; Sandhäger, 2000; Grosfeld and Sandhäger, 2004) focuses on the consideration of fracture processes in ice shelf simulation. This poses several difficulties: the model is based on continuum-mechanical balance equations, while fractures represent discontinuities of the ice body; the horizontal model grid resolution of 1.25 km is too low to incorporate formation and propagation of individual cracks; adequate fracture and calving criteria are not yet available; established simulation approaches do not yet exist. Thus, our primary task is to develop a parameterisation scheme which enables identification of potential formation areas of fractures from the inherent stress field of the ice shelf and describes the influence of these fractures on the flow regime.

Since observations suggest a particular importance of pronounced shear zones (Rack et al., 1999; 2000), we tentatively formulated an associated fracture criterion. It assumes that shear fractures form in the ice body where maximum horizontal shear $|\tau_{\hat{x}\hat{y}|\max}|$ exceeds a critical threshold $\tau_{\hat{x}\hat{y}|\mathrm{crit}}$ ($\tau_{\hat{x}\hat{y}|\max}$ is the shear with respect to the bisecting lines of the principal horizontal axes). To simulate the influence of a shear zone on the ice shelf flow, we impose a local reduction in ice viscosity by providing the flow parameter A of Glen's law with an enhancement factor $m_\mathrm{f} > 1$. This factor increases with increasing ratio between fracture zone thickness H_f and total ice shelf thickness H. Considering that a shear zone can cause dynamical decoupling of adjoining ice body parts, we impose a reduction in horizontal shear deformation rate $\dot{\varepsilon}_{xy}$ by introducing a coupling factor $0 < \beta < 1$, proportional to thickness ratio H_f/H and surface temperature T_s. This approach associates shear zone activation with enhanced melt water infiltration, presupposing that the latter process directly depends on duration and intensity of the melt season and, thus, on surface temperatures. Besides formation of shear fractures, their advection due to the ice flow is simulated on the basis of the modelled horizontal ice velocity field $\vec{u} = (u, v)^\mathrm{T}$ and under the assumption of continuous 'healing', which lasts longest in the case of maximum shear zone thickness (i.e., $H_\mathrm{f} = H$) and is completed after a total time t_heal. Tidal flexure at the grounding line is assessed as an additional relevant process, leading to a local reduction in ice shelf viscosity. Thus, we provide the flow parameter A with an second enhancement factor $m_\mathrm{gl} > 1$.

With regard to a regular Cartesian x, y, z-coordinate system the governing equations of ice shelf flow to be implemented in the advanced version of COMB*IS*^{2}S read:

$$2\frac{\partial}{\partial x}\left((F+F_\mathrm{f})\dot{\varepsilon}_{xx}\right)+\frac{\partial}{\partial x}\left((F+F_\mathrm{f})\dot{\varepsilon}_{yy}\right)+\frac{\partial}{\partial y}\left((F+\beta F_\mathrm{f})\dot{\varepsilon}_{xy}\right)=\bar{\rho}gH\frac{\partial(h-H)}{\partial x}+g\frac{\partial}{\partial x}\left(\int_{h-H}^{h}\int_{z}^{h}\rho\,dz'\,dz''\right),$$

$$2\frac{\partial}{\partial y}\left((F+F_\mathrm{f})\dot{\varepsilon}_{yy}\right)+\frac{\partial}{\partial y}\left((F+F_\mathrm{f})\dot{\varepsilon}_{xx}\right)+\frac{\partial}{\partial x}\left((F+\beta F_\mathrm{f})\dot{\varepsilon}_{xy}\right)=\bar{\rho}gH\frac{\partial(h-H)}{\partial y}+g\frac{\partial}{\partial y}\left(\int_{h-H}^{h}\int_{z}^{h}\rho\,dz'\,dz''\right)$$

with

$$F=m_\mathrm{gl}\left(\int_{h-H}^{h-H_\mathrm{f}}A(T)^{-\frac{1}{n}}dz'\right)\dot{\varepsilon}^{\frac{1}{n}-1},\quad F_\mathrm{f}=\max(m_\mathrm{gl},m_\mathrm{f})\left(\int_{h-H_\mathrm{f}}^{h}A(T)^{-\frac{1}{n}}dz'\right)\dot{\varepsilon}_\mathrm{f}^{\frac{1}{n}-1},\quad \dot{\varepsilon}_{xx}=\frac{\partial u}{\partial x},\quad \dot{\varepsilon}_{yy}=\frac{\partial v}{\partial y},$$

$$\dot{\varepsilon}_{xy}=\frac{1}{2}\left(\frac{\partial u}{\partial y}+\frac{\partial v}{\partial x}\right),\quad \dot{\varepsilon}^2=\dot{\varepsilon}_{xx}^{\,2}+\dot{\varepsilon}_{yy}^{\,2}+\dot{\varepsilon}_{xx}\dot{\varepsilon}_{yy}+\dot{\varepsilon}_{xy}^{\,2},\quad \dot{\varepsilon}_\mathrm{f}^{\,2}=\dot{\varepsilon}_{xx}^{\,2}+\dot{\varepsilon}_{yy}^{\,2}+\dot{\varepsilon}_{xx}\dot{\varepsilon}_{yy}+\beta^2\dot{\varepsilon}_{xy}^{\,2},$$

where $\dot{\varepsilon}_{xx}$, $\dot{\varepsilon}_{yy}$ and $\dot{\varepsilon}_{xy}$ are the horizontal components of the strain rate tensor, $\dot{\varepsilon}$ is the effective strain rate, h the surface elevation above sea level, g the acceleration due to gravity, ρ the ice density, and T the ice temperature. The parameters $A(T)$ and n of Glen's flow law are predetermined as follows: the flow parameter $A(T)$ similar to the recommendations of Paterson (1994); the exponent n is equal to 3. The temperature distribution in the ice body is approximated by means of the simple relation $T(\tilde{z}) = (T_\mathrm{s} + \Delta T_\mathrm{s} - T_\mathrm{b})(\tilde{z}/H)^{1/3} + T_\mathrm{b}$ (instead of solving the heat transfer equation), where $\tilde{z}$ is the elevation above the ice shelf base and T_b the temperature at the base. The correction ΔT_s is a tuning parameter, accounting for advective heat transfer from the high-altitude catchment areas on the Antarctic Peninsula into Larsen B (cf., Scambos et al., 2000). The stress conditions in the ice body are determined by means of Glen's flow law from the strain rates. In combination with boundary values (for $\vec{u}$ at the grounding line; for the horizontal gradients of $\vec{u}$ at the ice front; for T at the surface and

bottom of the ice body), this set of model equations describes the distributions of the relevant ice dynamic quantities u, v, T, and $\tau_{xy|\max}$, subject to the respective ice body geometry.

The specification of the different model input quantities (Fig. 2) is based on various data sets. The digital terrain model describing the surface topography of Larsen B was deduced primarily from the data set provided by Bamber and Huybrechts (1996). This new terrain model was combined with the BEDMAP ice thickness model (Lythe et al., 2001) to get a hydrostatic relation and compatible density-depth profiles (Fig. 2 c). The hydrostatic relation, in turn, allowed a direct conversion of the terrain model into the corresponding digital ice thickness model (Fig. 2 a). The course of the grounding line and the velocities of glacier outflows result from SAR interferometry. Model boundary values for the mean annual surface temperature (Fig. 2 b) were chosen according to measurements at Matienzo Station (Rack, 2000) and the distribution represented by Vaughan and Doake (1996).

The different tuning parameters of the advanced model were carefully adjusted by means of a series of test runs, yielding the following specifications: $\Delta T_s = -3$ °C; $\tau_{xy|crit} = 87.5$ kPa; $5.5 \le m_f \le 10.5$ depending on H_f; $0.25 \le \beta \le 0.48$ depending on H_f and T_s; $t_{heal} = 65$ yr; $m_{gl} = 5.5$ in the immediate vicinity to the grounding line ($m_{gl} = 1$ elsewhere).

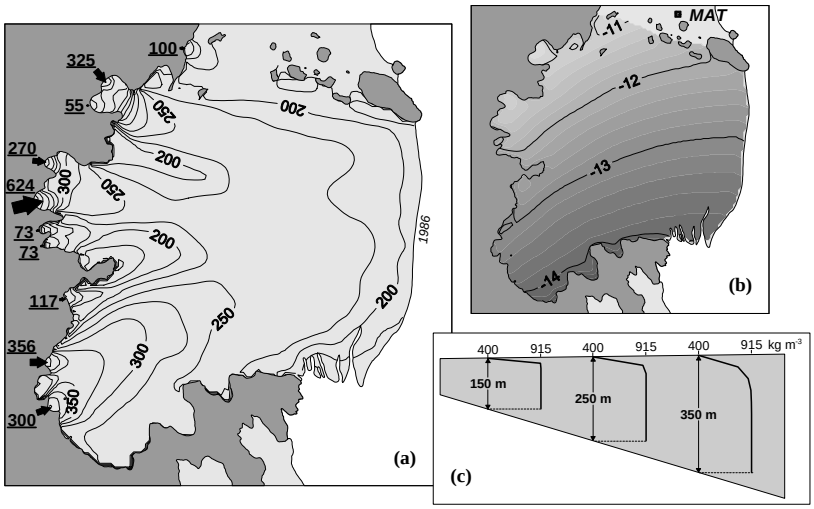

Figure 2: Specification of main input quantities for the numerical simulations of the Larsen B ice dynamics: (**a**) ice thickness distribution (m), velocities of glacier outflows (m yr^{-1}), grounding line position, 1986 ice front position; (**b**) mean annual surface temperatures (°C; MAT, Matienzo Station); (**c**) density − depth profiles for different ice thicknesses.

Reference and Configuration Runs for the 1986 stage of Larsen B

The flow regime of Larsen B simulated with the conventional model is characterized by a reasonable flow line pattern, but ice shelf velocities are too low by around 200 m yr^{-1} (Fig. 3 a, c, d; Reference Run). This model approach obviously tends to overestimate the dynamical coupling of the main ice shelf sections to the surrounding inland and the stagnant ice around Seal Nunataks. As expected, the velocity field obtained with the advanced model version agrees considerably better with observations (Fig. 3 b, c, d; Configuration Run). Since decoupling of ice body parts separated by pronounced shear zones as well as fracture-induced and tidal-induced ice shelf softening are now considered, the model reproduces the large velocity gradients at the ice shelf margins and near the glacier outflows.

A comparison between the simulated distribution of shear zones and the pattern of surface features visible in a RADARSAT image of Larsen B (Fig. 4) illustrates the potential of the new parameterisation scheme to identify many of the real fracture zones. Considerable discrepancies are found for the areas south of Seal Nunataks and east of Cape Disappointment, where the satellite image shows pronounced crevasses and rifts. They probably formed due to large tensile stress and, thus, cannot be identified by means of our fracture criterion based on a shear stress analysis. Although number, extensions and depths of simulated shear zones are apparently larger than inferred from observations, the Configuration Run reproduces basic characteristics of the former Larsen B flow regime. This is particularly evident from Figure 5, where synthetic interferograms for the ice velocities

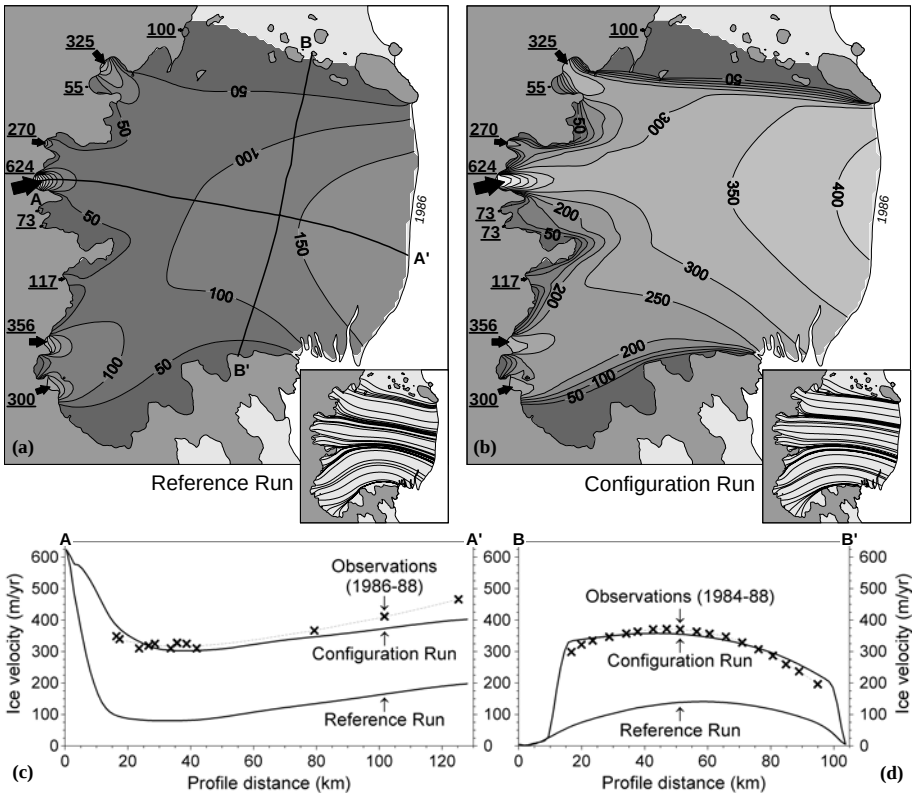

Figure 3: Modelled and measured velocities ($m\,yr^{-1}$) of the Larsen B ice flow in its stable 1986 configuration. (**a**), (**b**) Flow regimes as derived from the Reference Run using a conventional model approach and from the Configuration Run using the advanced model modules. The insets show associated flowline maps, indicating simulated directions of ice shelf flow. (**c**), (**d**) Comparison between modelled and measured ice velocities along the longitudinal profile A−A´ and the transversal profile B−B´. The positions of the profiles are marked in (a).

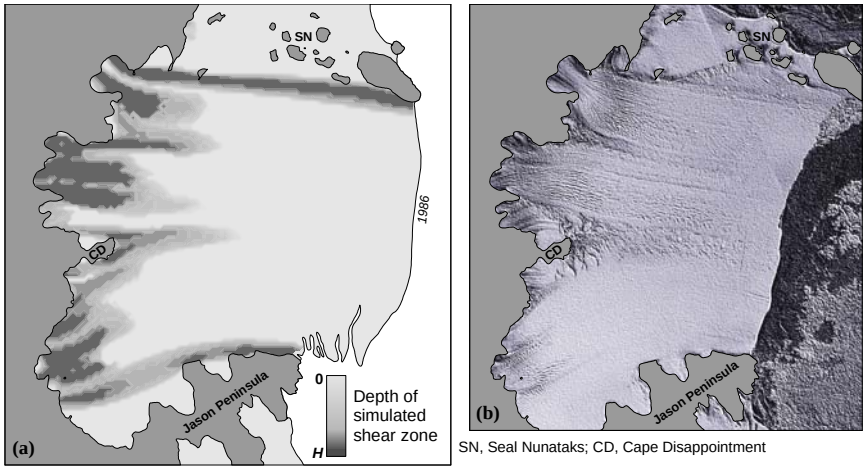

Figure 4: (**a**) Distribution of shear zones as simulated with the advanced ice shelf model. Dark-grey colouring indicates pronounced shear zones penetrating nearly the whole ice body. (**b**) Fractures and deformation features visible in a RADARSAT SAR image of Larsen B from 1997 (Jezek and RAMP Product Team, 2002).

resulting from the Reference and Configuration Runs are compared with a corresponding ERS SAR interferogram, which admittedly refers to the changed ice shelf stage on 16 / 17 November 1999. While the interferogram from the Reference Run shows a comparatively uniform fringe pattern, the interferogram from the Configuration Run comprises several differentiated structures similar to those visible in the real interferogram. This applies primarily to narrow fringe sequences related to zones of large velocity gradients. Poorly reproduced discontinuities in the fringe pattern again illustrate the deficiency of the advanced model in considering certain kinds of fractures and deformation features of

high ice dynamical relevance, such as crevasses, rifts, and cavitations on the leeside of ice rises and prominent inland parts. Nevertheless, we are confident that our advanced model together with the results of the Configuration Run provide a sufficiently reliable base for numerical experiments on the climate-induced retreat of Larsen B.

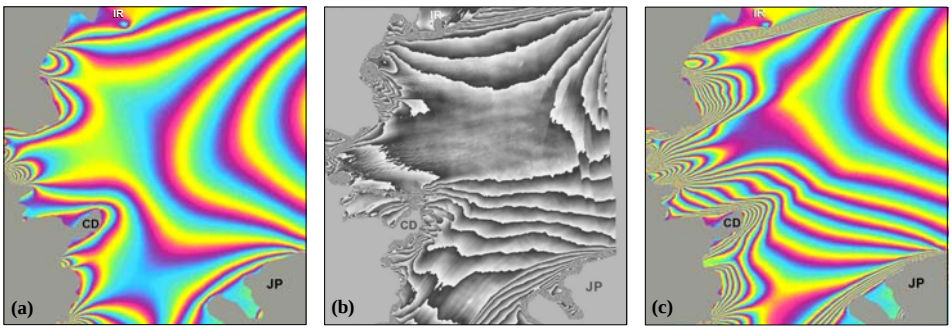

Figure 5: (**a**) Synthetic interferogram for ERS track 152, frame 4959, from ice velocities computed with the conventional model approach in the Reference Run. (**b**) ERS SAR interferogram of Larsen B (satellite track 152, 16 / 17 November 1995). (**c**) Synthetic interferogram from ice velocities computed with the advanced ice shelf model in the Configuration Run. IR, ice rise; CD, Cape Disappointment; JP, Jason Peninsula.

Sensitivity Runs

The first sensitivity experiment (Sensitivity Run 1995a) focuses on the Larsen B evolution from 1986 to the major calving event in late January 1995. We aim to evaluate whether the increase of ice shelf velocity between 1984 − 88 / 1986 − 88 and 1995 (Rack, 2000; cf., Fig. 7) mainly resulted from a reduction in the dynamical coupling along pre-existing fracture zones. A possible reason for a fracture activation like this could have been enhanced infiltration of melt water as a consequence of increased summer melt due to the atmospheric warming trend (Rott et al., 1998; Skvarca et al., 1999; Scambos et al., 2000; 2004). Since ice front position only changed little between 1986 and pre-calving stage in early 1995 (cf., Fig. 1 b), we performed the model experiment with the same geometrical setting as used for the Configuration Run. Furthermore, we retained the simulated distribution of shear zones (Fig. 4 a), but allowed for enlargement by newly identified formation areas. Reducing the coupling factor β by 0.15 (i.e., $0.10 \leq \beta \leq 0.33$ depending on H_f and T_s), the Sensitivity Run 1995a yielded increased ice velocities by several $10\,\mathrm{m\,yr^{-1}}$ for most of Larsen B (Fig. 6 a), which roughly corresponds to the observed flow acceleration (Fig. 7). However, the measured 1995 velocity profiles shown in Figures 7 a, b were derived interferometrically from ERS SAR data of the post-calving configuration and, thus, are possibly not directly comparable to the results of the Sensitivity Run 1995a for the pre-calving configuration. Although the simulation overestimates the velocity increase in northern Larsen B and underestimates the flow acceleration in the south, the results clearly indicate that fracture zone activation due to enhanced melt water infiltration could have been a fundamental process in the preliminary phase of progressive ice shelf retreat, destabilising the ice shelf. Neither observations nor the model results point to appreciable formation of new fracture zones during this transitional period from 1986 to early 1995.

The Sensitivity Run 1995b aims to assess possible consequences of the major calving event in late January 1995 for the Larsen B flow regime. Starting from the 1995a simulation and considering the calving-induced ice front retreat of 5 − 30 km, the model experiment shows a considerable decrease of the post-calving ice shelf velocities, which exceeds $100\,\mathrm{m\,yr^{-1}}$ in the north-eastern part of Larsen B (Fig. 6 b). On the whole, the modelled velocities are similar to those resulting from the Configuration Run (in spite of reduced dynamical coupling β), which suggests a stabilising effect of the 1995 calving event. This could explain the 4-year period of nearly unchanged Larsen B area following the calving event, before accelerated retreat started in 1999, which culminated in the collapse in February / March 2002 (Fig. 1 b). Although simulated post-calving velocities do not match the interferometrically derived values for 1995 (Fig. 7), this does not inevitably point to model deficiency. Since measured velocities are lacking for the pre-calving stage, it remains unclear, whether the 1995 calving event led to a deceleration of the ice shelf, preceded by a larger acceleration than supposed.

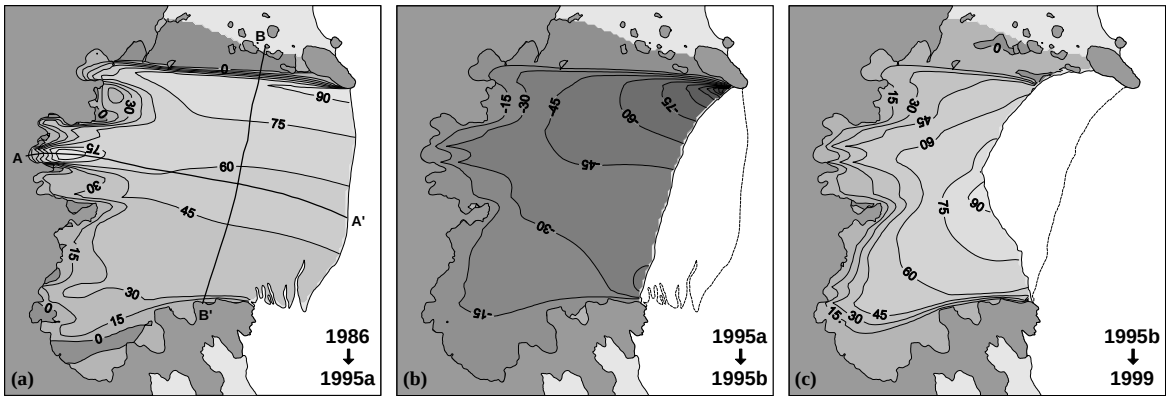

Figure 6: Simulated changes in ice velocities of Larsen B due to (**a**) enhanced dynamical decoupling along shear zones, (**b**) the major calving event in January 1995, and (**c**) further ice shelf retreat. The velocity differences are calculated from the results of the Configuration Run and the Sensitivity Runs 1995a, 1995b, and 1999, referring to the 1986 ice shelf stage, the 1995 pre-calving and post-calving stages, and the gradually retreating ice shelf in 1999, respectively. Positional changes of the ice front were comparatively small in the period from 1986 to early January 1995 and are neglected here.

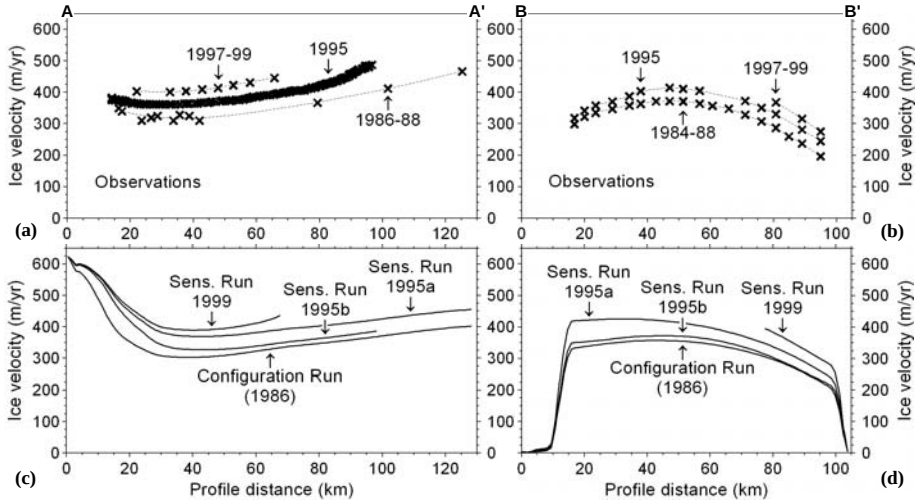

Figure 7: (**a**), (**b**) Ice velocities for different stages of Larsen B evolution derived from in situ measurements and satellite imagery along the longitudinal profile A−A´ and the transversal profile B−B´ (Rack, 2000; see Fig. 3 a, 6 a for profile positions). (**c**), (**d**) Corresponding velocity profiles extracted from the results of the model studies.

A detailed analysis of the results of the Sensitivity Run 1995b gave no indication why the ice shelf behaviour changed after the 1995 calving event from the previous pattern of multi-year advance to further retreat. However, observations suggest that a crucial process associated with this change was rift formation parallel to the ice front (Rott et al., 1998; Skvarca et al., 1999; cf., Fig. 4 b). A basic requirement for reliable simulations of the Larsen B ice dynamics during the transitional period from stable to unstable configuration is therefore the development of a more sophisticated model approach which considers additional forms of ice shelf fracturing, including particularly rifting and opening of large transverse crevasses.

The Sensitivity Run 1999 for an advanced stage of irreversible Larsen B retreat shows a substantial flow acceleration compared to the 1995 post-calving configuration (Fig. 6 c). The simulated velocity increase results primarily from the changed ice front position, but partly from shear zone deepening north of Jason Peninsula. A further reduction of the coupling factor β was not prescribed. Figure 7 shows that modelled and measured ice velocities largely agree along the remained parts of the longitudinal and transversal profiles A−A´ and B−B´. Since calving-induced flow acceleration can be interpreted as indication for unstable ice shelf behaviour, the results of the Sensitivity Runs are largely

consistent with the analysis of ice shelf stability performed by Doake et al. (1998) for the northern Larsen Ice Shelf. They showed that the 1995 calving event brought Larsen B close to its limit of stability and suggested that, if calving even of comparatively small icebergs continues, the ice shelf will decay until a new stable position is reached much closer to the inland. Such a (temporarily) stable configuration is possibly represented by the recent situation, where the only large remained part of Larsen B extends between Cape Disappointment and Jason Peninsula.

Conclusions

The numerical experiments emphasize that the flow regime of Larsen B, its climate sensitivity, and its evolution under atmospheric warming have been governed decisively by fracture processes in the body. Thus, a fundamental requirement for reliable ice shelf simulations is to consider these processes. We showed that the implementation of a relatively simple parameterisation scheme to identify potential shear zones and simulate their influences on the ice shelf flow already provides for an acceptable description of the Larsen B ice dynamics prior to its retreat and disintegration. However, this approach appeared to be inadequate to include fractures and deformation features formed primarily due to high tensile stresses, such as crevasses, rifts, and inlets. Despite these limitations, we even obtained plausible results from first applications of the advanced model to selected stages of changed ice shelf configuration. In particular, the model succeeded in simulating flow acceleration due to fracture zone activation and in identifying unstable ice shelf development, but it failed in reproducing the switch from stable to unstable ice shelf behaviour. We therefore plan to further improve the flow model by implementation of a more sophisticated fracture criterion based on additional stress components. This should facilitate innovative model experiments especially on the critical transitional period following the 1995 calving event and the rapid ice shelf collapse in February / March 2002. From these experiments we expect new insights into potential key mechanisms and processes related to climate-induced ice shelf disintegration. Furthermore, this would be an auspicious starting point for diagnostic and prognostic model studies for the major part of the Larsen Ice Shelf, i.e., the Larsen C.

References

Bamber, J.L. and P. Huybrechts (1996). Geometric boundary conditions for modelling the velocity field of the Antarctic ice sheet. *Ann. Glaciol*. **23**, 364-373.

Doake, C.S.M., H.F.J. Corr, H. Rott, P. Skvarca, and N.W. Young (1998). Breakup and conditions for stability of the northern Larsen Ice Shelf. Antarctica. *Nature* **391**, 778-780.

Grosfeld, K. and H. Sandhäger (2004). The evolution of a coupled ice shelf – ocean system under different climate states. *Global and Planetary Change* **42**,107-132.

Jezek, K. and RAMP Product Team (2002). *RAMP AMM-1 SAR image mosaic of Antarctica*. Fairbanks, AK: Alaska SAR Facility, in association with the National Snow and Ice Data Center, Boulder, CO (digital media).

Lythe, M.B., D.G. Vaughan, and the BEDMAP Consortium (2001). BEDMAP: A new ice thickness and subglacial topographic model of Antarctica. *J. Geophys. Res*. **106** (B6), 11,335-11,351.

Paterson, W.S.B. (1994). *The Physics of Glaciers*. 3rd ed., Pergamon/Elsevier, Oxford.

Rack, W. (2000). *Dynamic behavior and disintegration of the northern Larsen Ice Shelf, Antarctic Peninsula.* PhD-thesis, Universität Innsbruck, Austria.

Rack, W. and H. Rott (2004). Pattern of retreat and disintegration of Larsen B Ice Shelf, Antarctic Peninsula. *Ann. Glaciol*. **39**, (in press).

Rack, W., H. Rott, A. Siegel and P. Skvarca (1999). The motion field of northern Larsen Ice Shelf derived from satellite imagery. *Ann. Glaciol.* **29**, 261-266.

Rack, W., C.S.M. Doake, H. Rott, A. Siegel and P. Skvarca (2000). Interferometric analysis of the deformation pattern of the northern Larsen Ice Shelf, Antarctic Peninsula, compared to field measurements and numerical modelling. *Ann. Glaciol*. **31**, 205-210.

Rott, H., P. Skvarca and T. Nagler (1996). Rapid collapse of northern Larsen Ice Shelf, Antarctica. *Science* **271**, 788-792.

Rott, H., W. Rack, T. Nagler and P. Skvarca (1998). Climatically induced retreat and collapse of northern Larsen Ice Shelf, Antarctic Peninsula. *Ann. Glaciol.* **27**, 86-92.

Sandhäger, H. (2000). *Quantifizierung eisdynamischer und massenhaushaltsrelevanter Basisgrößen eines antarktischen Inlandeis-Schelfeis-Systems unter Einsatz eines numerischen Fließmodells*. PhD-thesis, Universität Münster, Germany.

Scambos, T.A., C. Hulbe, M. Fahnestock and J. Bohlander (2000). The link between climate warming and break-up of ice shelves in the Antarctic Peninsula. *J. Glaciol.* **46** (154), 516-530.

Scambos, T.A., C. Hulbe and M. Fahnestock (2004). Climate-induced ice shelf disintegration in the Antarctic Peninsula. In: Domack, E., A. Leventer, A. Burnett, R. Bindschadler, P. Convey and M. Kirby (eds.), *Anatarctic Peninsula Climate Variability: Historical and Paleoenvironmental Perspectives*, Ant. Res. Ser. **79**, American Geophysical Union, 79-92.

Skvarca, P., W. Rack, H. Rott and T. Ibarzábal-Donángelo (1998). Evidence of recent climate warming on the eastern Antarctic Peninsula. *Ann. Glaciol.* **27**, 628-632.

Skvarca, P., W. Rack and H. Rott (1999). 34 year satellite time series to monitor characteristics, extent and dynamics of Larsen B, Antarctic Peninsula. *Ann. Glaciol.* **29**, 255-260.

Vaughan, D.G. and C.S.M. Doake (1996). Recent atmospheric warming and retreat of ice shelves on the Antarctic Peninsula. *Nature* **379**, 328-331.